

Numerical Approach of Evaluating the Performance of Polymer Concentration and Adsorption to Enhance Frontal Advancement During Injection

Nelson Obi Duruodunze^a, Ifeanyi Samson Nwankwo^{a,b}, Bright Bariakpoa Kinate^{a,*}

^aDepartment of Petroleum Engineering, Rivers State University, Port Harcourt, Nigeria

^bDepartment of Petroleum Engineering, African University of Science and Technology, Abuja, Nigeria

Article

Article history
Received: 01 August 2021
Received in revised form:
31 August 2021
Accepted: 19 September
2021

Keywords:
Polymer,
Frontal Advance,
Grid,
Simulation,
Concentration,
Adsorption

Abstract

This work presents a numerical simulation approach in evaluating concentration and adsorption of polymer during a polymer flooding using a 3-D composite reservoir model with 100 cells (10x10x1). The reservoir was produced with two wells – injection (INJ) and producer (PROD) which are positioned at (3, 3, 1) and (8,8,1) grids respectively. The parameters investigated are the polymer adsorption coefficients, polymer in solution, oil/water saturation, oil-water capillary pressure and field production outputs. An increase in the amount of polymer (in solution) and the resulting polymer concentration and adsorption was fast in the producer grid cell (3, 3, 1) and slow in the grids at the extreme ends – (1, 1, 1) and (10, 10, 1). The presence of high permeability streaks along the central axis of the diagonal grid cells influences the polymer concentration distribution and adsorption. Hence, despite the equal spatial differences of grid cells (1,1,1) and (5, 5, 1) from the injector grid at (3, 3, 1), the amount of polymer in solution and the actual polymer concentration were far apart and not comparable. In the absence of reservoir fractures (or heterogeneity), advancement of polymer in water phase is relatively subject to the location of the injection well and the producer well.

1. Introduction

World energy forecast has shown that the demand for oil is ever increasing and would continue for near decades to come owing to its biggest contribution to the global energy needs. Oil with 32.9% of the global energy consumption is the world's leading fuel, while other sources of energy such as renewable in power generation and nuclear power grew below average rates [1]. It is therefore very necessary to recoup the vast available oil reserves from the entire producing reservoir while also exploring for new fields [2].

The growing worldwide energy demand is an indication that many hydrocarbons reserves such as proved undeveloped reserves (conventional or unconventional) will have to developed with available

*Corresponding author at: Department of Petroleum Engineering, Rivers State University, Port Harcourt, Nigeria
Email address: Kinate.bright@ust.edu.ng

or newer technologies. As of 2018, the world's total proven reserves was estimated at 1,498 billion barrels [3]. The development of conventional oil reserves is basically by natural depletion (primary recovery) and secondary recovery mechanisms. However, these techniques can be often limited by several factors such as reservoir and fluid properties, which could leave around 70% of the oil in the reservoir. To recover the large fraction of unrecovered oil, enhance oil recovery (EOR) is needed hence it is assumed necessary in most oil fields. The rise in energy demand globally has necessitated the venture into the development of these reserves using chemical process since they are not recoverable using conventional practice. More so, the extraction of hydrocarbon from unconventional reserves could significantly contribute in offsetting the growing world energy demand [4, 5].

Chemical recovery process is an effective EOR process that has significantly contributed to global daily oil production. Chemical EOR has been considered a productive oil recovery method capable of recovering residual oil trapped and/or bypassed in the reservoir. Chemical EOR method is based on the principle of injecting specially formulated chemicals (usually polymers, surfactants, etc) to increase oil recovery by increasing the injection fluid (water) potency [6]. The low cost and recorded success stories of its applications in varying fields across the globe makes them very appealing EOR method [7]. Samanta et al. (2012) identified the most widely used chemical EOR methods to include polymer injection, surfactant and alkaline flooding [8]. For 40 years now, polymer flooding has been identified as the most widely used chemical EOR method used in hydrocarbon recovery [9]. These chemicals are regularly screened in the laboratory to ascertain its performance potential since each chemical has a direct influence on oil production [10-12]. Recent studies have also shown that better mobility control, stability and consequently, improved oil recovery can be achieved via the use of foam enhanced by surfactants and polymers [13, 14]. The advent of nanotechnology with other fluids such as polymer and its application to increase the productivity of various processes in different fields has stimulated its use in the oil and gas industry [15-18]. Nanotechnology has shown positive improvements in addressing some problems in the oil and gas industry related to drilling operations, petroleum exploration, gas hydrate formation, EOR and hydraulic fracturing jobs [15, 19-21]. Nanofluid flooding has been assessed and analyzed with field application reported in Columbia as a chemical process [19]. Wettability alteration, improved viscosity of injectants and structural disjoining were established as the mechanism of the improved oil recovery [22].

In recent time, the use of high concentration and high molecular weight polymers has been particularly noted for improving oil recovery. These polymers are usually characterized with strong viscoelastic effect which potentially reduces residual oil saturation at the end of water flooding operation. Some of various fields noted for successful implementation of polymer flooding include the Daqing oilfield (China), East Bodo reservoir and Pelican Lake field (Canada), Marmul field (Oman) [23]. Till date polymer flooding remains increasingly relevant in the energy market. The boost in Daqing field oil production up to 3000,000 bbl/day remains the most outstanding success of polymer flooding EOR technology [24]. To ensure optimal performance of polymer flooding for a candidate reservoir, it is necessary to predict and monitor the variations in the fluid front advance and distribution within the reservoir rock matrix. This study therefore seeks to investigate the phenomenon of frontal advancement and grid cell fluid distribution using numerical simulation technique. This aimed at providing a detailed insight into the underlying mechanism of in-situ fluid displacement and its effect on oil recovery.

2. Methodology

This study considers a composite 3D reservoir grid system with grid cell dimensions, 10x10x1 (100 grid cells). The case study reservoir was produced for 10 years using two wells – a production well located at (1, 8) grid cell and a polymer injection well at (3, 1) grid cell. Prediction of future performance in terms of polymer frontal advance was made using a time step of 10 days to facilitate reduced

computational time over a 10 years production forecast. Analyses were made with respect to the reservoir grids associated with the wells [(1, 8) and (3,1)] so as to fully characterize and predict the performance of the polymer flooding project.

2.1. Mathematical Formulations

Manzoor (2020) developed a mathematical model for the flow of polymer that could be used to simulate the physics of the process of polymer flooding technique [25]. In the model the following assumptions were made:

- Energy exchange is neglected and fluid flow is isothermal.
- Only two fluid phases (oleic and aqueous) in three species (oil, water and polymer) are present in the throughout the system
- There is thermal equilibrium between the oleic and aqueous phases and the oil phase (typically heavy oil) is not dissolved in the polymer solution.
- There is no chemical and biological reaction between the species – oil, water and polymer.
- Polymer adsorption takes place on the solid matrix inside the cylindrical core, resulting from the bulk flow and dispersion mechanism of the mass transport.
- The bulk flow is along the z-direction, and flow is governed by Darcy’s law in a porous medium.
- The bulk flow (due to diffusion) across the radial direction is neglected.
- The density of the oil phase is kept constant throughout the process.
- The porous media has uniform porosity and permeability. Hence, gravity and capillary pressure effects are negligible.

From the underlying assumptions above, the resulting models are given in the equations below:

a. For Aqueous Phase

$$\begin{aligned} \frac{\partial S_w}{\partial t} = & \frac{KK_{rw}}{R_k\mu_p\phi} \left[\frac{\partial^2 p}{\partial z^2} \right] \\ & + \left[\frac{K}{R_k\mu_p\phi} \left(\frac{n_w K_{rw,ro}}{1 - S_{wc} - S_{or}} \right) \left(\frac{S_w - S_{wc}}{1 - S_{wc} - S_{or}} \right)^{n_w-1} \frac{\partial S_w}{\partial z} \frac{\partial P}{\partial z} + \frac{KK_{rw}}{R_k\mu_p\phi} C_w \frac{\partial^2 P}{\partial z^2} \right. \\ & - \frac{KK_{rw}}{R_k\mu_p\phi} \frac{\partial P}{\partial z} \frac{\partial C}{\partial z} \left(\frac{(R_{kmax} b_{rk} - b_{rk})}{R_k(1 + b_{rk} \cdot C)^2} \right) \\ & \left. + \left(\frac{(\mu_w a p_1 + 2\mu_w a p_2 \cdot C + 3\mu_w a p_3 \cdot C^2)}{\mu_p} \right) \right] \end{aligned} \quad (1)$$

b. For Oil Phase

$$\frac{\partial S_o}{\partial t} = \frac{KK_{ro}}{\mu_o\phi} \left[\frac{\partial^2 P}{\partial z^2} \right] + \left[\frac{K}{\mu_o\phi} \left(\frac{n_o K_{ro,ow}}{1 - S_{wc} - S_{or}} \right) \left(\frac{S_o - S_{or}}{1 - S_{wc} - S_{or}} \right)^{n_o-1} \frac{\partial S_o}{\partial z} \frac{\partial P}{\partial z} + \frac{KK_{ro}}{\mu_o\phi} C_o \frac{\partial^2 P}{\partial z^2} \right] \quad (2)$$

The resulting pressure and polymer concentration distribution are shown in the Equations (3) and (4):

$$\begin{aligned} \frac{\partial P}{\partial t} = & \frac{KK_{ro}}{\mu_o \phi C_T} \left[\frac{\partial^2 p}{\partial z^2} \right] + \left[\frac{K}{\mu_o \phi C_T} \left(\frac{n_o K_{ro,cw}}{1 - S_{wc} - S_{or}} \right) \left(\frac{S_o - S_{or}}{1 - S_{wc} - S_{or}} \right)^{n_o - 1} \frac{\partial S_o}{\partial z} \frac{\partial P}{\partial z} \right] + \frac{KK_{rw}}{R_k \mu_p \phi C_T} \left[\frac{\partial^2 P}{\partial z^2} \right] \\ & + \left[\frac{K}{R_k \mu_p \phi C_T} \left(\frac{n_w K_{rw,ro}}{1 - S_{wc} - S_{or}} \right) \left(\frac{S_w - S_{wc}}{1 - S_{wc} - S_{or}} \right)^{n_w - 1} \frac{\partial S_w}{\partial z} \frac{\partial P}{\partial z} \right. \\ & - \frac{KK_{rw}}{R_k \mu_p \phi C_T} \frac{\partial C}{\partial z} \frac{\partial P}{\partial z} \left(\left(\frac{R_{kmax} b_{rk} - b_{rk}}{R_k (1 + b_{rk} \cdot C)^2} \right) \right. \\ & \left. \left. + \left(\frac{(\mu_w \alpha p_1 + 2\mu_w \alpha p_2 \cdot C + 3\mu_w \alpha p_3 \cdot C^2)}{\mu_p} \right) \right) \right] \end{aligned} \quad (3)$$

$$\begin{aligned} \frac{\partial C}{\partial t} = & Df_a \left[\frac{\partial^2 C}{\partial z^2} \right] + \frac{Df_a \phi_t C_R}{\phi} \frac{\partial C}{\partial z} \frac{\partial P}{\partial z} + \frac{KK_{rw} C}{R_k \mu_p \phi} \left[\frac{\partial^2 P}{\partial z^2} \right] \\ & + \left[\frac{KC}{R_k \mu_p \phi} \left(\frac{n_w K_{rw,ro}}{1 - S_{wc} - S_{or}} \right) \left(\frac{S_w - S_{wc}}{1 - S_{wc} - S_{or}} \right)^{n_w - 1} \frac{\partial S_w}{\partial z} \frac{\partial P}{\partial z} \right. \\ & - \frac{KK_{rw} C}{R_k \mu_p \phi} \left(\frac{\partial C}{\partial z} \right) \left(\frac{\partial P}{\partial z} \right) \left(\left(\frac{R_{kmax} b_{rk} - b_{rk}}{R_k (1 + b_{rk} \cdot C)^2} \right) \right. \\ & \left. \left. + \left(\frac{(\mu_w \alpha p_1 + 2\mu_w \alpha p_2 \cdot C + 3\mu_w \alpha p_3 \cdot C^2)}{\mu_p} \right) \right) \right] \end{aligned} \quad (4)$$

where:

R_k = permeability reduction factor, R_{kmax} = maximum permeability reduction factor, b_{rk} = permeability reduction parameter, μ_p, μ_w = viscosity of polymer and aqueous solution respectively (PaS), ϕ = porosity, η_w = index of water relative permeability (dimensionless), K_{rw0} = oil relative permeability at irreducible water saturation, K_{rw} = water relative permeability, S_{or} = residual oil saturation (fraction), S_{wc} = residual water saturation (fraction), S_w, S_o = water and oil saturations respectively, C_w = compressibility factor of water (1/Pa), C_T = total compressibility factor (1/Pa), $\alpha p_1, \alpha p_2, \alpha p_3$ = viscosity parameters, μ_o = viscosity of oil (PaS), η_o = index of oil relative permeability, $K_{ro,cw}$ = water relative permeability at residual oil saturation, C_o = compressibility factor of oil (1/Pa), C_r = total compressibility (1/Pa), D = diffusion coefficient of polymer in free solution (m^2/s), C = polymer concentration.

The above equations (3-4) consider the combined effects of polymer concentration on solution viscosity, permeability reduction, and inaccessible pore volume to enhance heavy-oil production in polymer flooding using constant and time-varying injection pressure as well as solvent concentration.

- **Permeability Reduction Factor**

The term residual resistance factor (RRF) can be used to correlate the reservoir permeability reduction factor. It is a dimensionless variable mathematically defined as:

$$RRF = \frac{\Delta P_{WF \text{ before polymer flooding}}}{\Delta P_{WF \text{ after polymer flooding}}} \quad (5)$$

This mathematical statement is an indication that permeability reduction is created during polymer flooding. Using an analytical approach, permeability reduction factor (F_{kr}) can be ordinarily expressed in Equation (6) as follows:

$$F_{kr} = 1 + (F_{kr,max} - 1) \frac{C_p}{AdC} \quad (6)$$

where $F_{kr,max}$, dimensionless is the maximum permeability reduction factor, AdC is the maximum adsorption capacity ($gmol/m^3$) and C_p is the residual adsorption level ($gmol/m^3$).

2.2. Simulation Approach

In this study, a stepwise algorithm/ simulation flow chart presented in Figure 1 was used to ensure consistent results with model description. The study deploys a Schlumberger Eclipse 100 black oil model (fully implicit mode) [26].

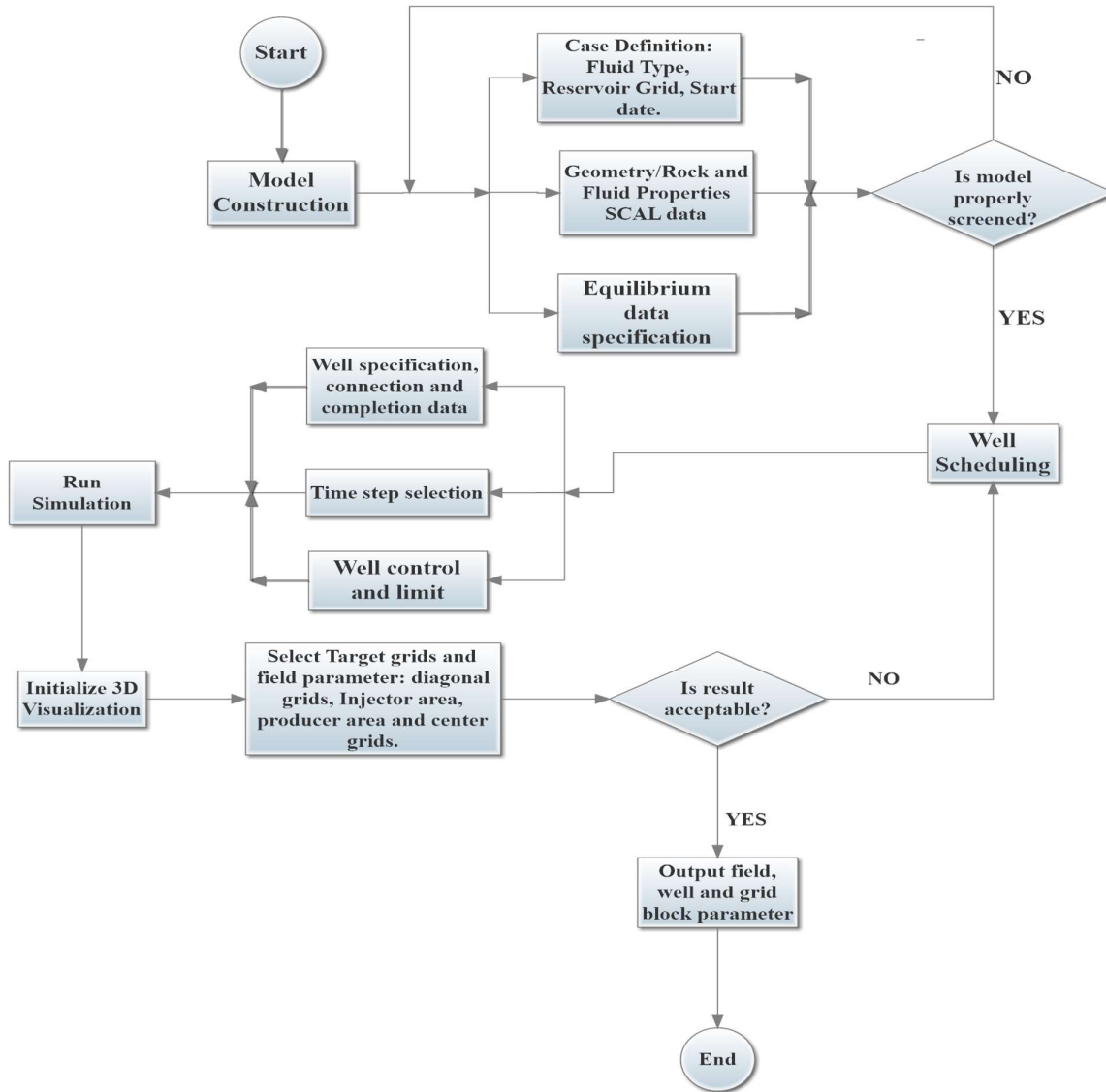


Figure 1. Simulation flow chart

The key assumptions employed are stated as follows:

- The reservoir system is anisotropic and homogenous in x, y and z-directions
- The external bounds of the reservoir are sealed
- The polymer injector, INJ1(3,3) injects at constant rate
- The change in fluid mobility varies across the reservoir grids
- The reservoir is produced isothermally
- There is no mass transfer between the fluid phases

The case study description, reservoir grid definition and well schedule for producer and injector are presented in Tables 1, 2 and 3. The i and j location of the injector and producer were selected to minimize boundary effects and possible impact of mobility challenges created by the high permeability streaks at

the center grids. The diagonal axis of the grid layout represents the shortest distance of injector-producer well spacing of the entire reservoir.

Table 1. Case Definition

S/N	Parameter	Description
1	Reservoir Type	Ordinary Black Oil Reservoir
2	Equation of State	Peng Robinson
3	Phases Present	Oil, water and polymer
4	Simulation Start Date	21st December, 2020
5	Reservoir Model	Cartesian (Block Centered)

Table 2. Reservoir Grid Definitions

S/N	Property	Description/Unit
Grid type	Cartesian (Block Centered)	Ft
Grid Dimension	10x10x1	
Number of Cells	100	
PERMX	50	Md
PERMY	50	5md
PERMZ	5	Md
Porosity	0.2	Fraction
Dx	75	Ft
Dy	75	Ft
Dz	30	Ft
NTG Ratio	1	Dimensionless
TOPS	4000	Ft

Table 3. Well Completion Scheduling of the Producer and the Injector Wells

Location/Control Parameter	INJ1	PROD1
i-location	3	8
j-location	3	8
k-upper	1	1
k-lower	1	1
Preferred Phase	Polymer	Oil
Well type	Injector	Producer
Well Control Mode	Liquid Rate/BHP	BHP
Wellbore radius	0.33ft	0.33ft

3. Results and Discussion

The 3-D Reservoir X model comprising of 100 grid cells, 10x10x1 with central grids, (4, 4, 1), (5, 5, 1) and (6, 6, 1) having high permeability streaks caused by fractures is shown in Figure 2. To get a closest approximate to the reservoir geometry, Eclipse keyword, ACTINUM, was used to deactivate the cells that were considerably outside the reservoir geological model. The synthetic reservoir was then simulated over a 10years production period at a timestep of 10 days using two wells – an oil producer located at (8, 8, 1) and a polymer injector placed at (3, 3, 1). As shown in the reservoir grid layer out in Figure 1, both wells were placed two cells away from the reservoir boundary in order to minimize the possible boundary effects. Analyses were made with respect to the diagonal cells, (1, 1, 1), (2, 2, 1), (3, 3, 1), (4, 4, 1), (5, 5, 1), (6, 6, 1), (7, 7, 1), (8, 8, 1), (9, 9, 1) and (10, 10, 1). The core parameters considered are the polymer adsorption coefficients, polymer in solution, oil and water saturation, oil-water capillary pressure and field production outputs.

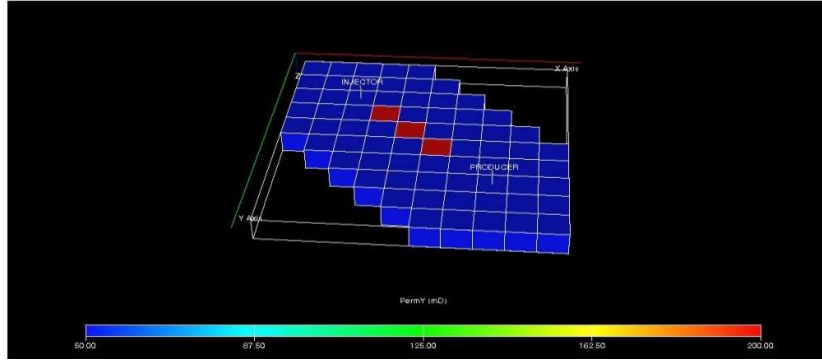


Figure 2. Reservoir X Grid Layout

3.1. Cell Polymer Propagation

The factors and variables considered in analyzing the polymer front advancement in the reservoir matrix are the polymer in solution, polymer adsorption and the resulting oil-water capillary pressure. The results as presented in Figures 3, 4, and 5 shows the cell polymer in solution, cell polymer concentration and cell polymer adsorption of the diagonal cells. An increase in the amount of polymer in solution and the resulting polymer concentration and adsorption yields fast in the producer grid cell (3, 3, 1) and slow in the grids at the extreme ends (1, 1, 1) and (10, 10, 1). In addition, the presence of high permeability streaks along the central axis of the diagonal grid influences the polymer concentration distribution and adsorption. Hence, despite the equal spatial differences of grid cells (1, 1, 1) and (5, 5, 1) from the injector grid at (3, 3, 1), the amount of polymer in solution and the actual polymer concentration were far apart and not comparable.

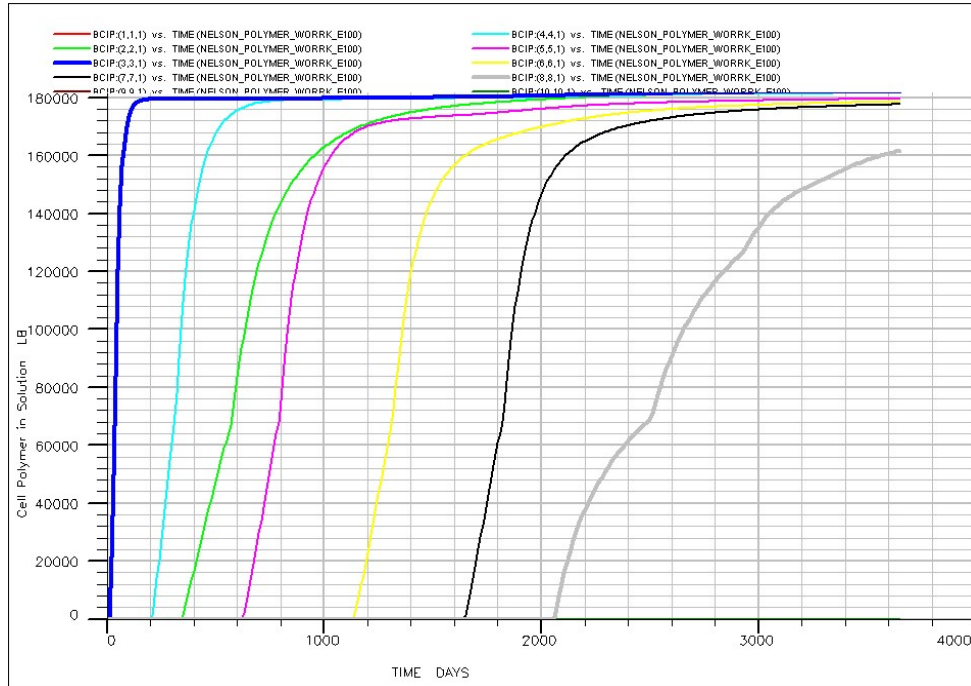


Figure 3. Grid Cell (Diagonal Grids) Polymer in Solution versus Time

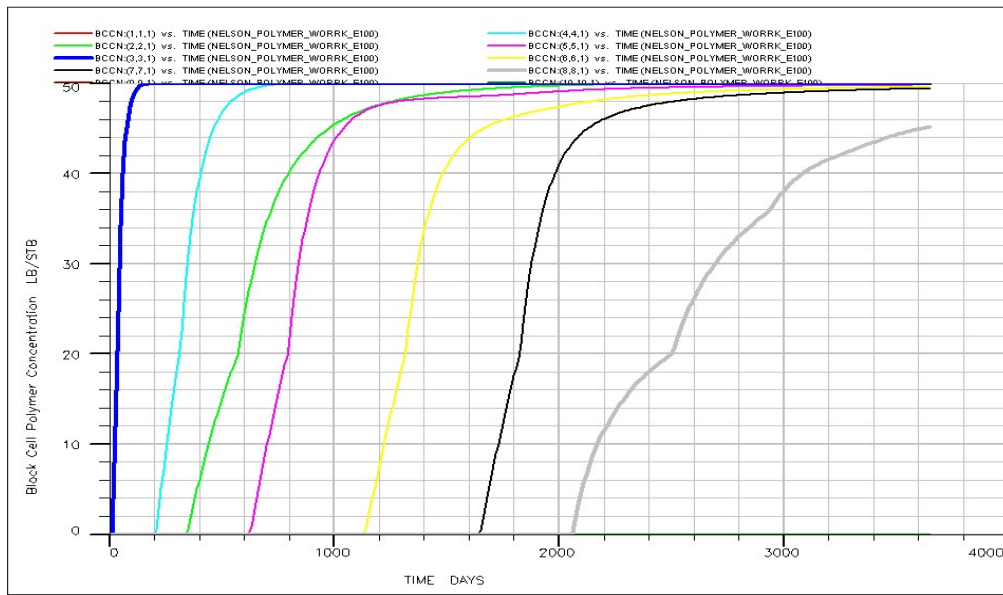


Figure 4. Grid Cell (Diagonal Grids) Polymer Concentration versus Time

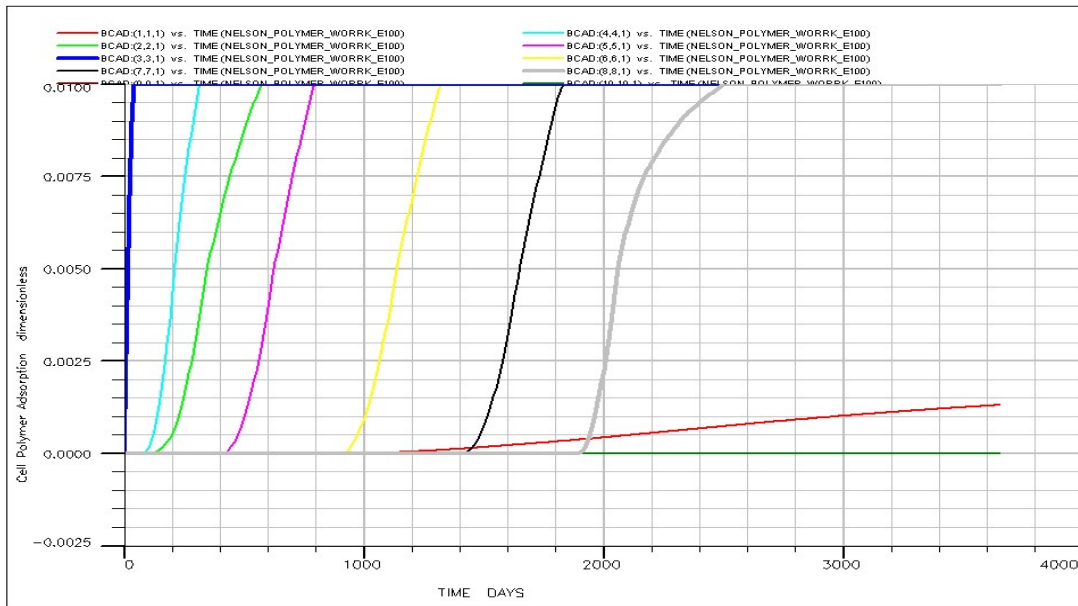
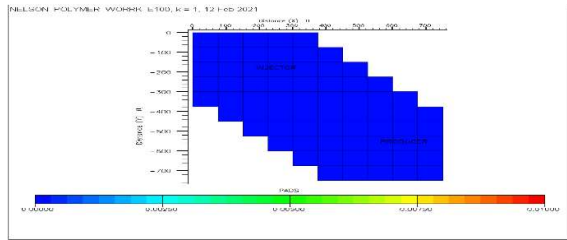


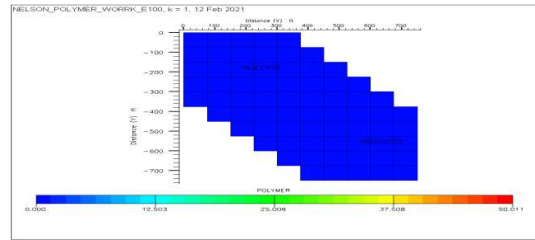
Figure 5. Grid Cell (Diagonal Grids) Polymer Adsorption versus Time

The result was affirmed by the grids in the immediate neighborhood of the injector well - (2, 2, 1) and (4, 4, 1) with a rapid change in the fractured grid cell, (4, 4, 1). Without reservoir fractures (or heterogeneity), the advance of polymer in water phase is relatively subject to the location of the injection well and the producer well which resulted to the minimal cell polymer adsorption in grid cell (9, 9, 1) and (10, 10, 1) as shown in Figure 5. Figure 6 shows a 2-D flow visualization at the start of production and at the end of 2nd, 3rd, 7th and 10th year (the end of production) production periods for the cell polymer adsorption and cell polymer concentration. The polymer adsorption in any cell is dependent on the amount of polymer in that cell. At the end of the first year, the aqueous polymer phase breaks through the fractured reservoir grid (4, 4, 1) which causes it to advance faster towards the producer well. Increment in polymer concentration along the diagonal grids influences the polymer adsorption (PADS) on the left.

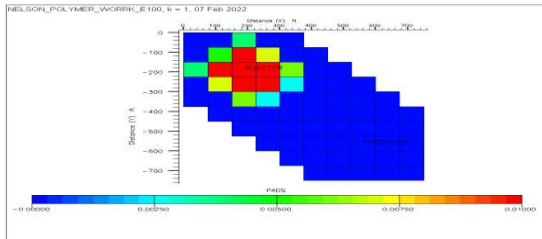
The resulting oil and water saturations with their sweep efficiency are presented in Figure 7. The remarkable residual oil saturation at the extreme grids indicates that moving the wells one grid apart will result more oil recovering from the reservoir.



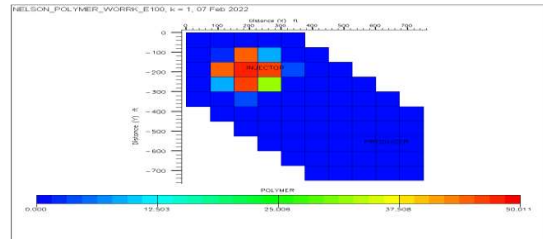
Start of Production (PADS)



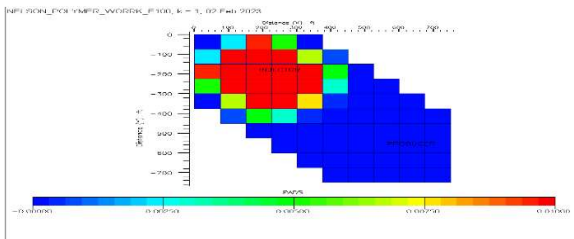
Start of Production (POLYMER)



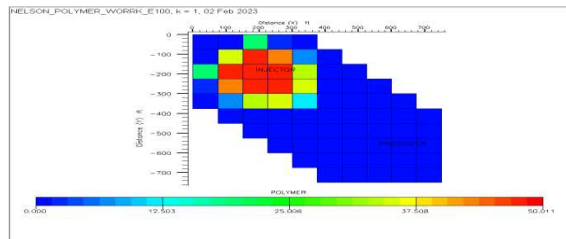
At the end of first year (PADS)



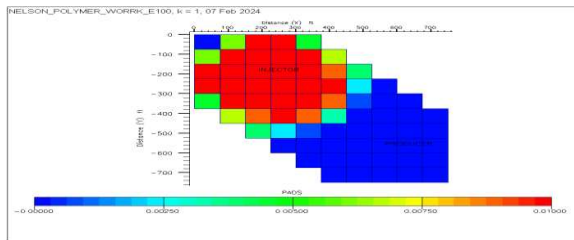
At the end of first year (POLYMER)



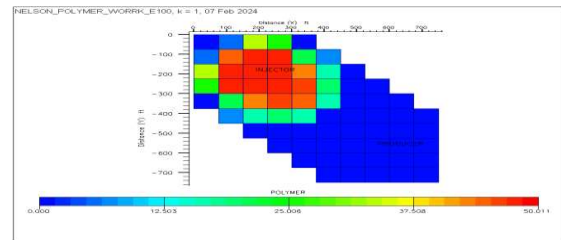
At the end of second year (PADS)



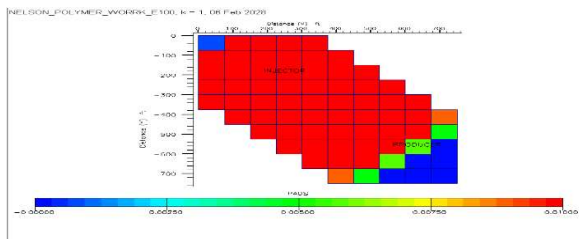
At the end of second year (POLYMER)



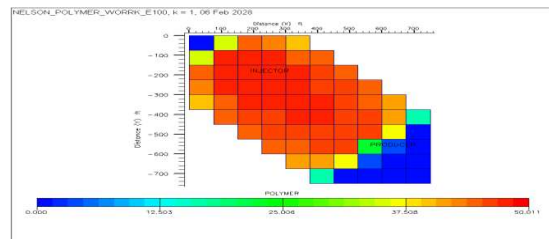
At the end of third year (PADS)



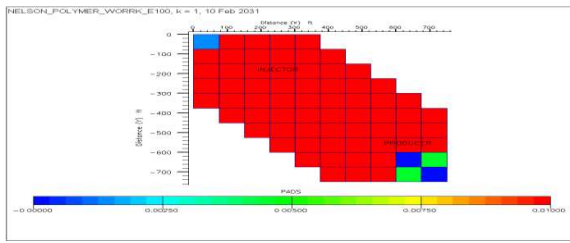
At the end of third year (POLYMER)



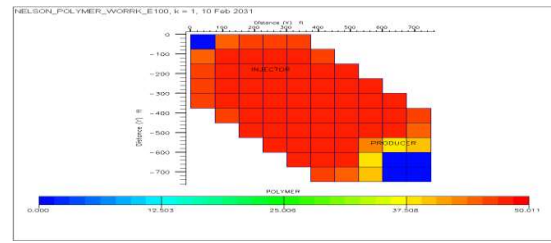
At the end of seventh year (PADS)



At the end of seventh year (POLYMER)

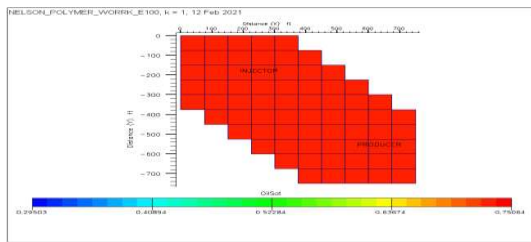


At the end of tenth year (PADS)

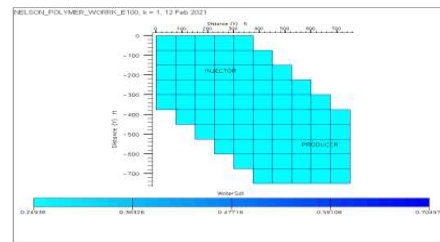


At the end of tenth (POLYMER)

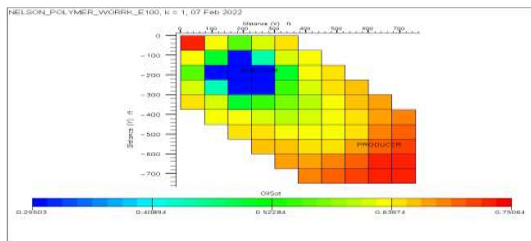
Figure 6. Grid Cell Polymer Adsorption (PADS) and Polymer Concentration (POLYMER) Variations Over the Period



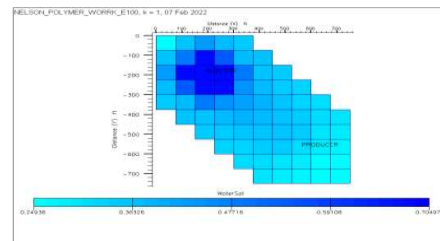
SOIL - Start of production



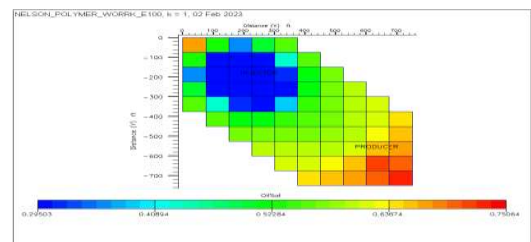
SWAT - Start of production



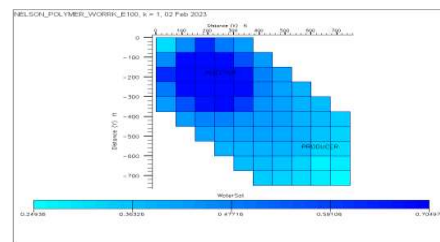
SOIL - At the end of first year



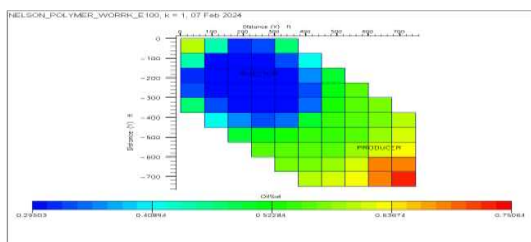
SWAT - At the end of first year



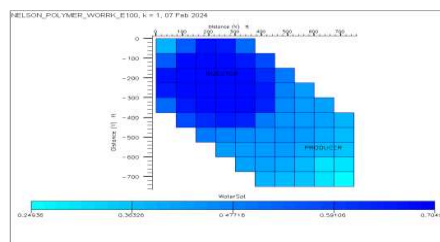
SOIL - At the end of second year



SWAT - At the end of second year



SOIL - At the end of third year



SWAT - At the end of third year

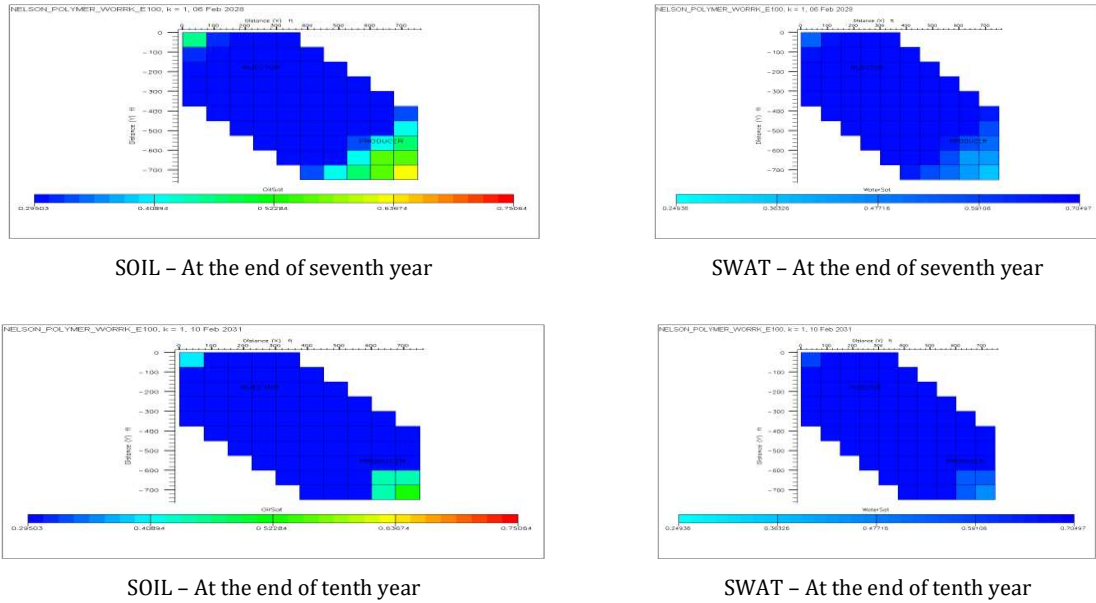


Figure 7. Grid Cell Oil Saturation (SOIL) and Water Saturation (SWAT) Variations Over the Period

3.2. Reservoir Performance

The essence of any EOR technique is to maximize fluid recovery from the reservoir. The simulated field output from the Reservoir is presented in Figure 8 to Figure 11. The results of the field oil production potential (FOPP) showed that after 3000 days of production, the potential field useful life was exhausted and the field produces at rates less than 5 STB/day.

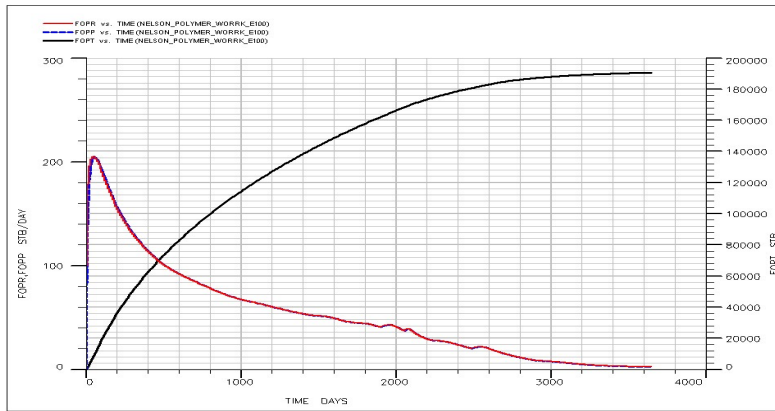


Figure 8. Field Oil Production Rate and Production Potential

Injecting at constant rate increases the polymer adsorption due to increased polymer deposition within the reservoir pores and results in pressure increment and a recovery factor of 0.58 as shown in Figure 9. The rate of adsorption increase if polymer is injected at higher rates until a maximum polymer adsorption is attained. Injecting at lower rates extend the duration at which maximum polymer adsorption is reached. The polymer been in aqueous phase with the water phase increases the field water cut to almost 100% at 3000 days of production. This validates the assumption that the field's useful life may have been exhausted at this point.

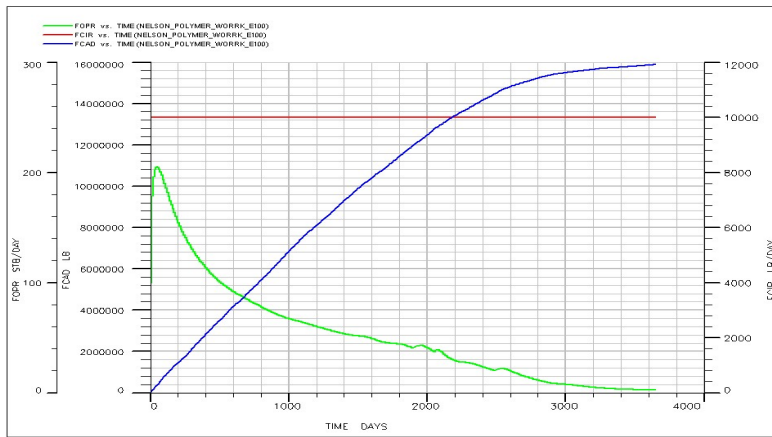


Figure 9. Field Oil Production Rate with Polymer Injection Rate and Adsorption in the Reservoir Rock Matrix

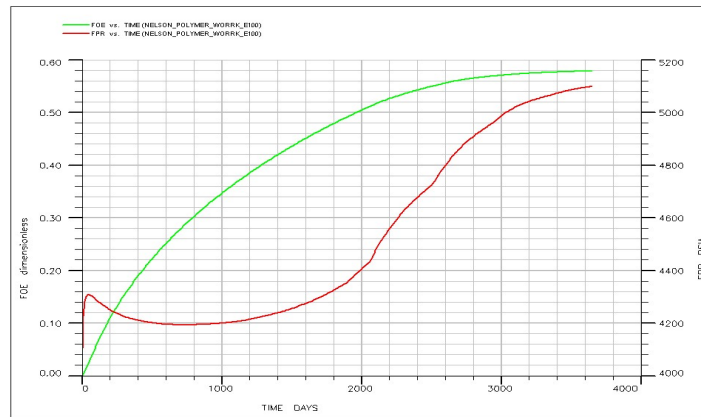


Figure 10. Field Recovery Factor and Field Pressure versus Time

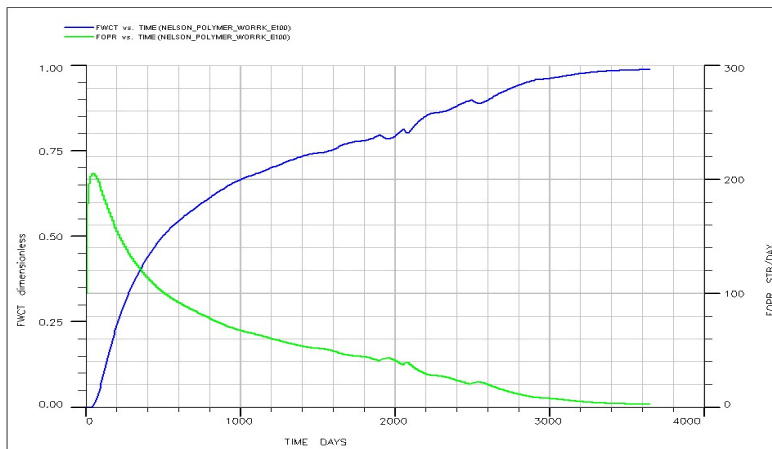


Figure 11. Field Water Cut and Field Oil Production Rate versus Time

3.3. The Effect of Polymer Injection on Oil Flow

The influence of the INJECTOR on the oil – water saturation, oil – water capillary pressure, relative permeability to oil and the grid cell pressure distribution is presented in Figure 12 to 17. Spatial differences results to decline in the oil saturation in grids (1, 1, 1), (9, 9, 1) and (10, 10, 1). Similar trend occurs for the water saturation history. In addition, at the end of the period of investigation, the residual

oil saturation was 30% with a corresponding water saturation of 70% for the other grid cells apart from grids (1, 1, 1), (9, 9, 1) and (10, 10, 1).

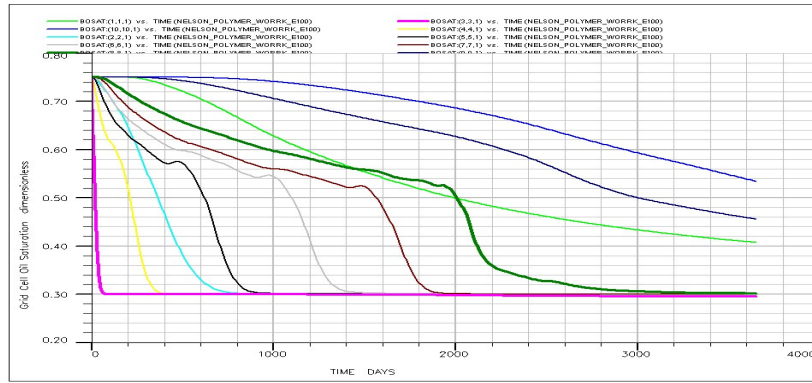


Figure 12. Grid block Oil Saturation Profile

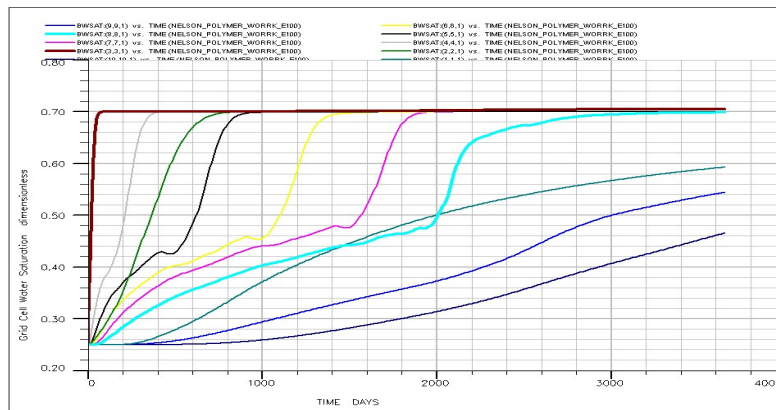


Figure 13. Diagonal Grid Cell Water Saturation History

Figure 14 shows the oil-water saturation of the producer and the injector grid cell. After about 2000 days of production, the water saturation equals the oil saturation for the grid cell, (8, 8, 1) bearing the producer. In the injector well grid (3, 3, 1), the water saturation far exceeds the oil saturation just after the production was initiated. This is attributed to the effect of the polymer injection, which is actually in water phase. The oil–water capillary pressure and relative permeability to oil also follow the same trend as seen in Figure 15 and 16. The capillary pressure change observed explained the alteration of interfacial tension of the in-situ oil and the water phase mobility reduction.

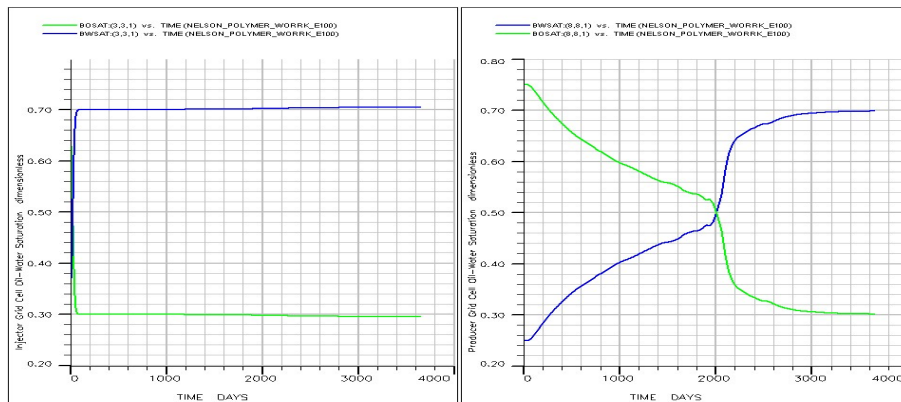


Figure 14. Injector and Producer Grid Cell Oil-Water Saturation

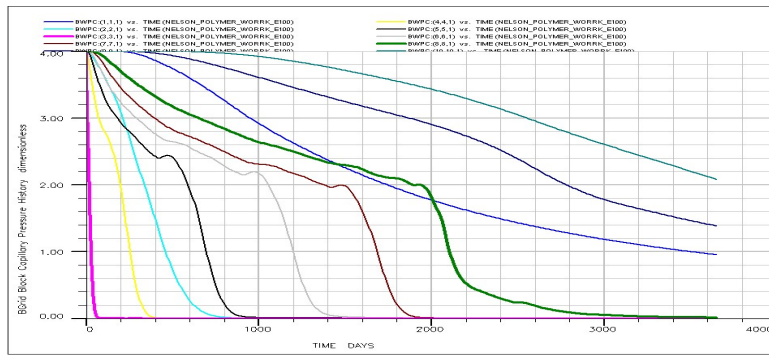


Figure 15. Diagonal Grid Cells Water-Oil Capillary Pressure History

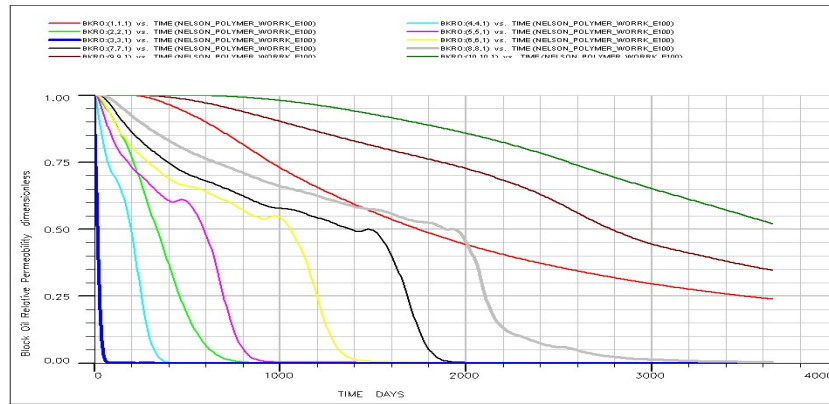


Figure 16. Diagonal Grids Relative Permeability to Oil

The pressure distribution of the diagonal grids as seen in Figure 17 shows a low-pressure distribution in the producer grid cell caused by the withdrawal (oil production) which creates a pressure drop especially in the immediate vicinity of the well grid cells and advances towards the reservoir boundary following a typical pressure transient path. However, further effect of the pressure drop caused by the production activities in grid cell (8, 8, 1) was inhibited by the injection well at (3, 3, 1) such that there was a continuous pressure build up in each of the reservoir grid cells with highest pressure build up at the injection well cell

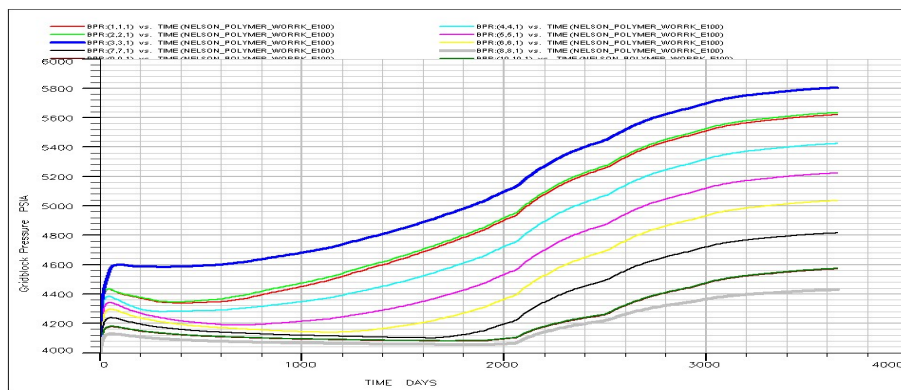


Figure 17. Selected Grid Blocks (Diagonal Grids) Pressure Distribution

3.4. Well Productivity Index and Bottomhole Pressure History

With a constant rate of polymer injection, the bottomhole pressure was constant which resulted in a constant well productivity (injectivity) index for the injector well after an initial reduction as shown in Figure 18. This initial reduction is due to the effect of porous filling often experienced at the onset of

injection activities. The non-uniform trend of the well productivity index (WPI) and well bottom hole pressure (WBHP) seen in the producer well illustrates the effect of rate changes (drop) over the period of production. The sharp drop of WPI of the producer (PRODUCER) at 2000 days of production rescinded the fact that oil saturation has dropped below 50% which gives more room for increased water production/ water cut as presented in Figure 19.

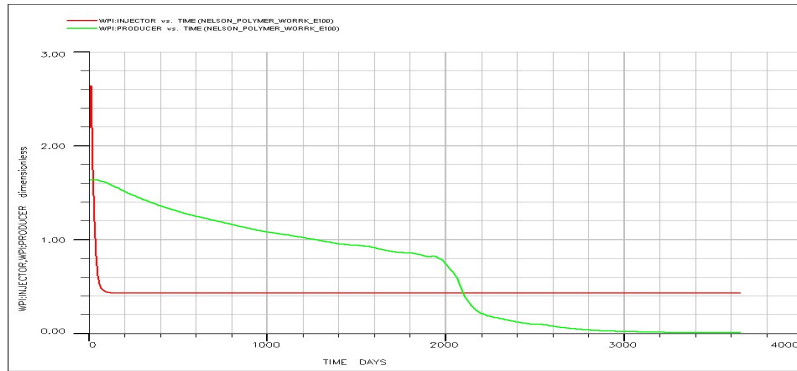


Figure 18. Injector and Producer Well Productivity Index

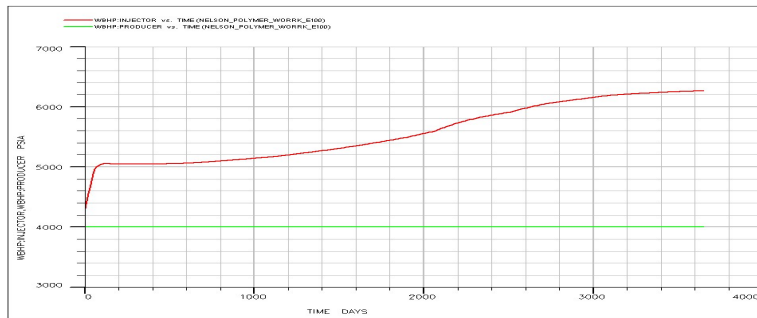


Figure 19. Injector and Producer Well Bottomhole Pressure Profile

4. Conclusion

This study adopted numerical method to evaluate the performance of polymer adsorption and concentration for frontal advancement during the polymer injection. A black oil reservoir simulator (ECLIPSE 100) was used to analyze the effect of polymer concentration and injection on reservoir performance and well productivity index. Prediction of future performance of polymer frontal advancement was made using a time step of 10 days to facilitate reduced computational time for over a 10 years production with the following conclusion.

- Increase in the amount of polymer in solution and the resulting polymer concentration and adsorption was faster in the injector grid cell (3, 3, 1) and slow in the grids at the extreme ends (1, 1, 1) and (10, 10, 1).
- Injecting at a constant high rate increases the adsorption due to increased polymer deposition within the reservoir pores and kept the bottomhole pressure constant with increase in recovery factor
- Lower rate injection extends the duration of maximum polymer adsorption
- Relative spacing between the production well and polymer injector has critical effect on the area sweep efficiency of the injected polymer.
- Optimal well spacing (distance between injector and producer) is vital for maximum recovery with polymer injection

References

- [1] BP: Statistical Review of World Energy in Review, (2019).
- [2] Al Adasani A., Bai B.: Analysis of EOR projects and updated screening criteria. *Journal of Petroleum Science and Engineering*, **79**, 10-24 (2011). DOI: <https://doi.org/10.1016/j.petrol.2011.07.005>
- [3] OPEC: Annual Statistical Bulletin: Viena, Australia (2019).
- [4] Conti J., Holtberg P.: *International Energy Outlook. Independent Statistics & Analysis*, U.S. Energy information Administration DOE/EIA-0484, (2011).
- [5] Conti J., Holtberg P., Diefenderfer J., LaRose A., Turnure J. T., Westfall L.: *International energy outlook 2016 with projections to 2040*, USDOE Energy Information Administration (EIA), Washington, DC (United States ... (2016).
- [6] Baviere M.: Basic concepts in enhanced oil recovery processes. (1991).
- [7] Levitt D., Pope G. A.: Selection and Screening of Polymers for Enhanced-Oil Recovery. in *SPE Symposium on Improved Oil Recovery*. (2008 of Conference). DOI: [10.2118/113845-MS](https://doi.org/10.2118/113845-MS)
- [8] Samanta A., Bera A., Ojha K., Mandal A.: Comparative studies on enhanced oil recovery by alkali-surfactant and polymer flooding. *Journal of Petroleum Exploration and Production Technology*, **2**, 67-74 (2012). DOI: [10.1007/s13202-012-0021-2](https://doi.org/10.1007/s13202-012-0021-2)
- [9] Pope G. A.: Recent Developments and Remaining Challenges of Enhanced Oil Recovery. *Journal of Petroleum Technology*, **63**, 65-68 (2011). DOI: [10.2118/0711-0065-IPT](https://doi.org/10.2118/0711-0065-IPT)
- [10] Iglauer S., Rahman T., Sarmadivaleh M., Al-Hinai A., Fernø M. A., Lebedev M.: Influence of Wettability on Residual Gas Trapping and Enhanced Oil Recovery in Three-Phase Flow: A Pore-Scale Analysis by Use of Microcomputed Tomography. *SPE Journal*, **21**, 1916-1929 (2016). DOI: [10.2118/179727-PA](https://doi.org/10.2118/179727-PA)
- [11] Iglauer S., Wu Y., Shuler P., Tang Y., Goddard W. A.: Alkyl polyglycoside surfactant-alcohol cosolvent formulations for improved oil recovery. *Colloids and Surfaces A: Physicochemical and Engineering Aspects*, **339**, 48-59 (2009). DOI: <https://doi.org/10.1016/j.colsurfa.2009.01.015>
- [12] Schramm L. L.: *Surfactants: fundamentals and applications in the petroleum industry*, Cambridge university press (2000).
- [13] Kumar A., Mandal A.: Synthesis and physicochemical characterization of zwitterionic surfactant for application in enhanced oil recovery. *Journal of Molecular Liquids*, **243**, 61-71 (2017). DOI: <https://doi.org/10.1016/j.molliq.2017.08.032>
- [14] Zaitoun A., Makakou P., Blin N., Al-Maamari R. S. S., Al-Hashmi A. R. R., Abdel-Goad M., Al-Sharji H. H. H.: Shear Stability of EOR Polymers. *SPE Journal*, **17**, 335-339 (2012). DOI: [10.2118/141113-PA](https://doi.org/10.2118/141113-PA)
- [15] Khoja A. H., Tahir M., Amin N. A. S.: Cold plasma dielectric barrier discharge reactor for dry reforming of methane over Ni/ γ -Al₂O₃-MgO nanocomposite. *Fuel Processing Technology*, **178**, 166-179 (2018). DOI: <https://doi.org/10.1016/j.fuproc.2018.05.030>
- [16] Ko S., Huh C.: Use of nanoparticles for oil production applications. *Journal of Petroleum Science and Engineering*, **172**, 97-114 (2019). DOI: <https://doi.org/10.1016/j.petrol.2018.09.051>
- [17] Yousefvand H., Jafari A.: Enhanced Oil Recovery Using Polymer/nanosilica. *Procedia Materials Science*, **11**, 565-570 (2015). DOI: <https://doi.org/10.1016/j.mspro.2015.11.068>
- [18] Krishnamoorti R.: Technology Tomorrow: Extracting the Benefits of Nanotechnology for the Oil Industry. *Journal of Petroleum Technology*, **58**, 24-26 (2006). DOI: [10.2118/1106-0024-IPT](https://doi.org/10.2118/1106-0024-IPT)
- [19] Agi A., Junin R., Gbadamosi A.: Mechanism governing nanoparticle flow behaviour in porous media: insight for enhanced oil recovery applications. *International Nano Letters*, **8**, 49-77 (2018). DOI: [10.1007/s40089-018-0237-3](https://doi.org/10.1007/s40089-018-0237-3)
- [20] Gbadamosi A. O., Junin R., Manan M. A., Yekeen N., Augustine A.: Hybrid suspension of polymer and nanoparticles for enhanced oil recovery. *Polymer Bulletin*, **76**, 6193-6230 (2019). DOI: [10.1007/s00289-019-02713-2](https://doi.org/10.1007/s00289-019-02713-2)
- [21] Gbadamosi A. O., Kiwalabye J., Junin R., Augustine A.: A review of gas enhanced oil recovery schemes used in the North Sea. *Journal of Petroleum Exploration and Production Technology*, **8**, 1373-1387 (2018). DOI: [10.1007/s13202-018-0451-6](https://doi.org/10.1007/s13202-018-0451-6)
- [22] Franco C. A., Zabala R., Cortés F. B.: Nanotechnology applied to the enhancement of oil and gas productivity and recovery of Colombian fields. *Journal of Petroleum Science and Engineering*, **157**, 39-55 (2017). DOI: <https://doi.org/10.1016/j.petrol.2017.07.004>
- [23] Sheng J. J.: Chapter 3 - Polymer Flooding—Fundamentals and Field Cases, in *Enhanced Oil Recovery Field Case Studies*, J. J. Sheng, Editor Gulf Professional Publishing, Boston 63-82 (2013)
- [24] Cheraghian G., Hendraningrat L.: A review on applications of nanotechnology in the enhanced oil recovery part A: effects of nanoparticles on interfacial tension. *International Nano Letters*, **6**, 129-138 (2016). DOI: [10.1007/s40089-015-0173-4](https://doi.org/10.1007/s40089-015-0173-4)
- [25] Manzoor A. A.: Modeling and Simulation of Polymer Flooding with Time-Varying Injection Pressure. *ACS Omega*, **5**, 5258-5269 (2020). DOI: [10.1021/acsomega.9b04319](https://doi.org/10.1021/acsomega.9b04319)
- [26] Schlumberger: Eclipse office (2009).